



OPEN

Using U-Net convolutional neural network to model pixel-based electrostatic potential distributions in GaN power MIS-HEMTs

Bang-Ren Chen¹, Yu-Sheng Hsiao², Wei-Cheng Lin¹, Wen-Jay Lee³✉, Nan-Yow Chen³✉ & Tian-Li Wu^{1,2,4}✉

This study demonstrates a novel use of the U-Net convolutional neural network (CNN) for modeling pixel-based electrostatic potential distributions in GaN metal–insulator–semiconductor high-electron mobility transistors (MIS-HEMTs) with various gate and source field plate designs and drain voltages. The pixel-based images of the potential distribution are successfully modeled from the developed U-Net CNN with an error of less than 1% error relative to a TCAD simulated reference of a 500-V electrostatic potential distribution in the AlGaN/GaN interface. Furthermore, the modeling time of potential distributions by U-Net takes about 80 ms. Therefore, the U-Net CNN is a promising approach to efficiently model the pixel-based distributions characteristics in GaN power devices.

Keywords GaN HEMT, Electrostatic potential modeling, Machine learning, U-Net

Gallium nitride high electron mobility transistors (GaN HEMTs) are attractive due to two-dimensional electron gas (2DEG), large breakdown E-field, and the wide bandgap. Recently, thanks for the insulator under the gate metal, high performance power metal–insulator–semiconductor high electron mobility transistors (MIS-HEMTs) have been demonstrated^{1–3}, which is promising for the power switching applications. However, the high electrical field in the access region during an off-state drain bias stress can lead to the earlier breakdown, defect generations and trapping effects, limiting the performance and stability of these GaN HEMTs^{4,5}. To address these issues, field plates (FPs) have been designed to optimize the electrostatic potential^{6,7}; this is crucial for performance and reliability, particularly in GaN HEMTs for high-power applications. Numerical simulation techniques, such as technology computer-aided design (TCAD) simulations, have been widely used for modeling electrostatic potentials^{8,9}. However, these simulations are time-consuming because of the complexity of the heterojunction and underlying physics. Moreover, although analytical models are often used to model device electrical characteristics^{10,11}, analytical models cannot be efficiently applied to devices with different materials and structures.

Recently, high-performance computing has enabled the use of deep learning techniques to predict the electrical properties of devices from the input parameters^{12–17}. However, since fully connected neural networks are not designed for image-related tasks, electrostatic potential modeling in previous studies has been limited to one-dimensional devices¹². On the other hand, the convolutional neural network (CNN) based approach^{18–27} is also attractive for pixel-based image prediction and segmentation, which has been widely used in the biomedical sciences^{21,22,24,25} due to local connection and weight-sharing advantages. Still, the applications of CNN-based approach are limited in the semiconductor research. Recently, one study reported that the pixels of the two-dimensional landscape of low-voltage Si devices could be modeled by a CNN with a U-Net architecture²⁶. Note that the advantage of using a U-Net CNN is that, in general, U-Net CNN requires only few images to have a relatively good results^{23–27}. The network of U-Net is structured with a contracting path and an expansive path, forming its distinctive U-shaped architecture. The contracting path embodies a conventional convolutional network, utilizing a series of convolution applications, each paired with a rectified linear unit (ReLU) and a subsequent max pooling operation. This phase systematically diminishes spatial information while

¹International College of Semiconductor Technology, National Yang Ming Chiao Tung University, Hsinchu, Taiwan. ²Institute of Pioneer Semiconductor Innovation, National Yang Ming Chiao Tung University, Hsinchu, Taiwan. ³National Center for High-Performance Computing, Hsinchu, Taiwan. ⁴Institute of Electronics, National Yang Ming Chiao Tung University, Hsinchu, Taiwan. ✉email: wjlee@nchc.narl.org.tw; nanyow@nchc.narl.org.tw; tlwu@nycu.edu.tw

amplifying feature data. Conversely, the expansive pathway unites feature and spatial information by employing up-convolutions and merging them with high-resolution features obtained from the contracting path through concatenation. However, this work²⁶ is limited to the dimensional variation with only considering the impact of on-state voltage that directly applied at the surface of the semiconductor with simplified symmetric device design that is not practical for the real device fabrication, which results from the relative compact and shallow network constructed by only 4 layers of contracting path and the expanding path. Furthermore, the impacts of the external dimensional variations, e.g., field plate variations on top of the semiconductor, on the potential distribution inside the semiconductor are not discussed²⁶, which is more practical for the consideration of the semiconductor design.

In this work, we demonstrate U-Net CNN approach to model the pixel-based electrostatic potential image in GaN power MIS-HEMTs considering the different gate and source field plates and drain voltages, showing that the electrostatic potential can be accurately and effectively modeling by using the U-Net CNN approach. Our modified U-Net is consisted of 7 layers of the contracting path and 7 layers of the expanding path. Each contracting path is consisted of 2 convolutions with ReLU followed by a maxpooling function. Last two layers of the contracting path even followed by a dropout function in order to avoid the overfitting problem. On the other hand, each layer of the expanding path is consisted of a upsampling with ReLU, the concatenation with the data from the counterpart of the contracting path, and 2 convolutions with ReLU.

Device schematic and typical electrical property

Schematic of a GaN MIS-HEMT is shown in Fig. 1. The electrostatic potentials in this work are generated by Sentaurus TCAD for various gate and source field plate designs and different applied drain biases ranged from 100 to 500 V with a step of 100 V. The gate and source field plates are designed by considering the ratio compared to the gate-to-drain distance (L_{GD}) as shown in Eq. (1) & (2). Please note that the ratio of the gate and source field plates ranges from 0 to 1. The field plate designs used in this work are shown in Table 1.

$$\text{Gate field plate ratio} = \frac{L_{FP_{Gate}}}{L_{GD}} \quad (1)$$

$$\text{Source field plate ratio} = \frac{L_{FP_{Source.extra}}}{L_{Source.extra}} \quad (2)$$

A total of 80 images representing the electrostatic potential distribution were generated through TCAD simulations that ran for over 640 h. Figure 2 presents an example of the pixel-based images of electrostatic potential distribution generated from TCAD simulation with consideration of the gate FP ratio, source FP ratio, and drain voltage of 0.8, 0.8, and 500 V, respectively.

Methodology

Figure 3a presents the workflow for predicting the pixel-based electrostatic potential of the GaN MIS-HEMTs using a U-Net CNN model and schematics of the input layers. The images of device structures are divided into 6 layers to form the matrix representing the material information and applied voltage: (1) GaN, (2) AlGaIn, (3) AlN, (4) source/gate/drain metal, (5) nitride, and (6) the applied bias (Fig. 3b). For layers 1–5 in the one-hot

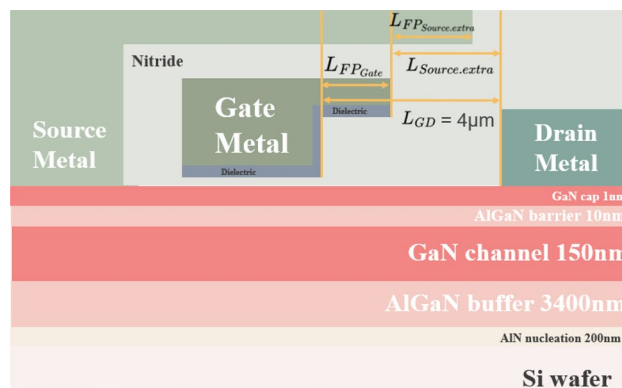


Figure 1. Schematic of the GaN MIS-HEMTs with the gate and drain field plate designs.

Gate field plate ratio	0.1	0.3	0.5	0.8
Source field plate ratio	0.1	0.3	0.5	0.8

Table 1. The field plate designs used in this work.

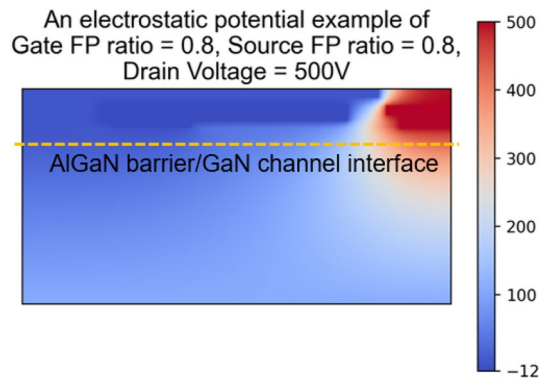


Figure 2. An example of the pixel-based images of electrostatic potential distribution generated from TCAD simulation.

matrix, if the pixel location is the targeted materials, it will be recorded as “1” or “0” for not the targeted materials. For the 6th layer, the voltage was linearly normalized to a range of 0–1.

The U-Net CNN consists of two segments: the down-sampling side and the up-sampling side as shown in Fig. 4. The down-sampling side contains eight rows of convolution and maxpooling. The up-sampling side contains eight rows of up-sampling, convolution, and concatenation. The model is trained and evaluated by the mean-squared error (MSE) loss function, which measures the error between the output electrostatic potentials from the developed U-Net CNN and the reference electrostatic potential from the TCAD simulations. The goal of the training process is to minimize the loss function by adjusting its parameters, resulting in the better modeling. The optimizer for the iterations is Adam algorithm with an initial learning rate of 5×10^{-6} . After the model is constructed, the images of the electrostatic potential distribution can be visualized for further verification.

The TCAD generated datasets are randomly divided into two groups: (1) the images for the training (72 images) and (2) the image for the verifications (8 images). The images for the verification purpose are not shown to the model during the training. Hence, they are suitable to verify the performance of the trained model.

Results and discussions

Figure 5 shows the decreases of the mean square error (MSE) during the training process, suggesting that developed U-Net CNN is efficient to minimize the error between the output electrostatic potentials from the developed U-Net model and the reference electrostatic potential from the TCAD simulations. Note that the TCAD computational environment is equipped with an 8 core Intel Xeon CPU, 47GiB of RAM, while the machine learning environment is equipped with a GPU of an Nvidia Tesla V100. Also, the training time of the U-Net CNN model is about 21.8 h.

Figure 6 shows the side-by-side comparison of the simulation results from the TCAD and the modeling results (output) from the trained U-Net model in the dataset of the image for verifications. Furthermore, a less than 1% error of the electrostatic potential distribution in AlGaIn/GaN interface can be obtained, indicating the excellent consistent results (Fig. 7). Furthermore, the modeling time of potential distributions by U-Net takes about 80 ms.

Conclusion

In this work, the modeling of the electrostatic potential distributions is successfully demonstrated for the first time by considering the pixel-base images using the U-Net CNN with the different gate and source field plate designs and applied drain voltages in GaN power MIS-HEMTs. The different gate and source field plate designs and drain voltages are generated by TCAD simulation as references in this study, and the corresponding pixel-based electrostatic potential distribution images are modeled by the U-Net CNN. Less than 1% error of a 500 V electrostatic potential modeling in the AlGaIn/GaN interface between the developed U-Net model and the reference electrostatic potential from the TCAD simulations can be achieved (error equation = $(U_{\text{simulation}} - U_{\text{U-Net}})/U_{\text{simulation}}$), indicating a successful modeling using developed U-Net CNN approach. Note that the modeling by the U-Net CNN requires only 80 ms, which is a huge speed improvement compared to the TCAD simulations. In sum, the U-Net CNN approach is promising for the accurate and efficient methodology in modeling the distribution-based characteristics, e.g., electrostatic potential, electric field, current density, etc., in GaN power devices.

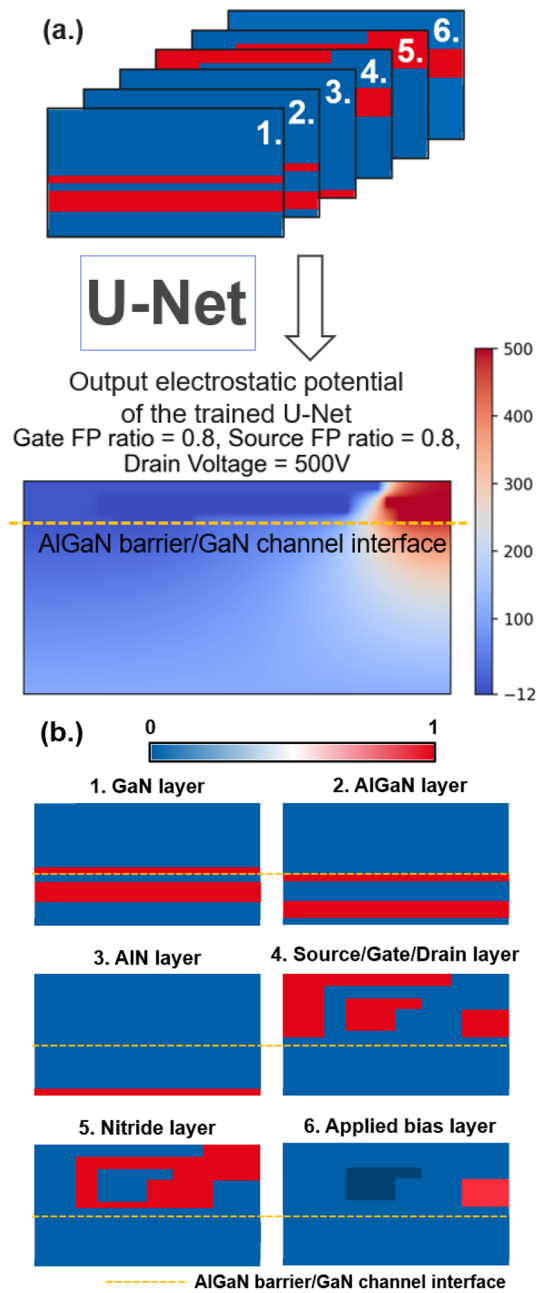


Figure 3. (a) An example of the electrostatic potential modeled by U-Net CNN and (b) the schematics of the 6 input layers.

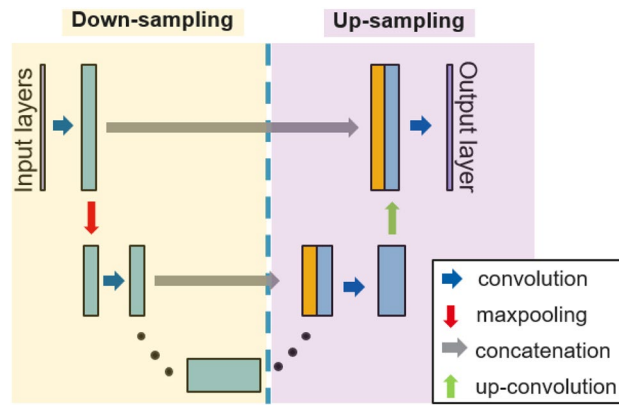


Figure 4. The simplified schematic of a U-Net model.

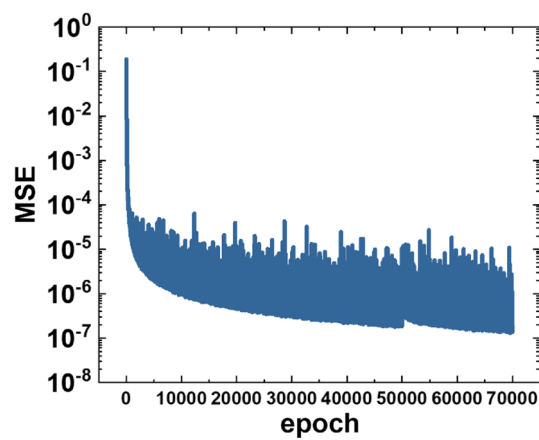


Figure 5. MSE records during the training process.

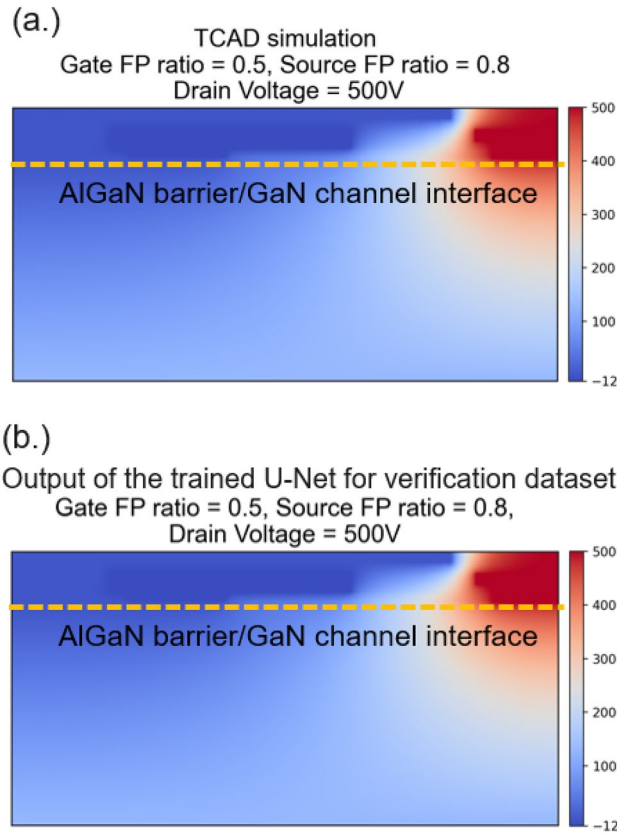


Figure 6. Comparison of electrostatic potential distributions from (a) the TCAD simulation and (b) the developed U-Net model.

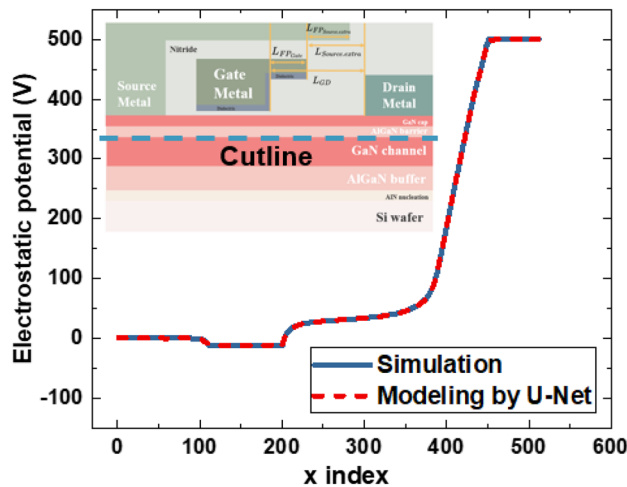


Figure 7. Comparison of electrostatic potential in AlGaIn/GaN interface from the TCAD simulation and the developed U-Net model.

Data availability

Data inquiries can be directed to the corresponding author.

Received: 9 September 2023; Accepted: 25 March 2024
 Published online: 08 April 2024

References

1. Van Hove, M. *et al.* CMOS process-compatible high-power low-leakage AlGaIn/GaN MISHEMT on silicon. *IEEE Electron Devices Lett.* **35**(5), 667–669. <https://doi.org/10.1109/LED.2012.2188016> (2012).
2. Liu, S.-C. *et al.* GaN MIS-HEMTs with nitrogen passivation for power device applications. *IEEE Electron Devices Lett.* **35**(10), 1001–1003. <https://doi.org/10.1109/LED.2014.2345130> (2014).
3. Moens, P., Liu, C., Banerjee, A., Vanmeerbeek, P., Coppens, P., Ziad, H., Constant, A., Li, Z., De Vleeschouwer, H., Roig-Guitart, J., Gassot, P., Bauwens, F., De Backer, E., Padmanabhan, B., Salih, A., Parsey, J. & Tack, M., An industrial process for 650V rated GaN-on-Si power devices using in-situ SiN as a gate dielectric. In Proc. IEEE 26th Int. Symp. Power Semiconductor Devices IC's (ISPSD), HI, USA, June 2014, <https://doi.org/10.1109/ISPSD.2014.6856054>.
4. Kobayashi, K. *et al.* Current collapse suppression in AlGaIn/GaN HEMTs by means of slant field plates fabricated by multi-layer SiCN. *Solid-State Electron.* **101**, 63–69 (2014).
5. Vetry, R., Zhang, N. Q., Keller, S. & Mishra, U. K. The impact of surface states on the DC and RF characteristics of AlGaIn/GaN HFETs. *IEEE Trans. Electron Devices* **48**(3), 560–566. <https://doi.org/10.1109/16.906451> (2001).
6. Karmalkar, S., Shur, M. S., Simin, G. & Khan, M. A. Field-plate engineering for HFETs. *IEEE Trans. Electron Devices* **52**(12), 2534–2540. <https://doi.org/10.1109/TED.2005.859568> (2005).
7. Miyamoto, H., Ando, Y., Okamoto, Y., Nakayama, T., Wakejima, A., Inoue, T., Murase, Y., Ota, K., Yamanoguchi, K., Kuroda, N., Tanomura, M., Matsunaga, K., AlGaIn/GaN field-plate FETs for microwave power applications. Gallium Nitride Materials and Devices II, 6473(647315, Jan. 2007, <https://doi.org/10.1117/12.707334>
8. Adak, S., Swain, S. K., Rahaman, H., Sarkar, C. K., Effect of doping in p-GaN gate on DC performances of AlGaIn/GaN normally-off scaled HFETs. In: 2017 Devices for Integrated Circuit (DevIC), Kalyani, India, 2017, pp. 372–375, <https://doi.org/10.1109/DEVIC.2017.8073972>.
9. Zhu, B., Bazizi, E. M., Tng, J.H.M., Li, Z., Banghart, E. K., Hassan, M. K., Hu, Y., Zhou, D., Choi, D., Qin, L., Wan, X., TCAD Simulation on FinFET n-type Power Device HCI Reliability Improvement. 2019 IEEE International Reliability Physics Symposium (IRPS), Monterey, CA, USA, 2019, pp. 1–4, <https://doi.org/10.1109/IRPS.2019.8720558>.
10. Nithin Kumar, N. R., & Vimala, P., Two Dimensional Analytical Potential Model for Double Gate TFETs. In: 2018 4th International Conference on Devices, Circuits and Systems (ICDCS), Coimbatore, India, 2018, pp. 241–244, <https://doi.org/10.1109/ICDCSyst.2018.8605141>.
11. Bhat, Z., & Aamir Ahsan, S., Physics-based Analytical Modeling of p-GaN/AlGaIn/GaN HEMTs. In: 2022 IEEE 19th India Council International Conference (INDICON), Kochi, India, 2022, pp. 1–6, <https://doi.org/10.1109/INDICON56171.2022.10039804>.
12. Han, S.-C., & Hong, S.-M., Deep Neural Network for Generation of the Initial Electrostatic Potential Profile. In: 2019 International Conference on Simulation of Semiconductor Processes and Devices (SISPAD), Udine, Italy, 2019, pp. 1–4, <https://doi.org/10.1109/SISPAD.2019.8870521>.
13. Wu, T.-L. & Bin Kutub, S. Machine learning-based statistical approach to analyze process dependencies on threshold voltage in recessed gate AlGaIn/GaN MIS-HEMTs. *IEEE Trans. Electron Devices* <https://doi.org/10.1109/TED.2020.3032634> (2020).
14. Bin Kutub, S., Jiang, H.-J., Chen, N.-Y., Lee, W.-J., Jui, C.-Y., & Wu, T.-L., Artificial Neural Network-Based (ANN) Approach for Characteristics Modeling and Prediction in GaN-on-Si Power Devices. In: Proc. IEEE 26th Int. Symp. Power Semiconductor Devices IC's (ISPSD), 2020. <https://doi.org/10.1109/ISPSD46842.2020.9170110>
15. Teo, C. W., Low, K. L., Narang, V., & Thean, A. V. Y., TCAD-Enabled machine learning defect prediction to accelerate advanced semiconductor device failure analysis. In: Proc. International Conference on Simulation of Semiconductor Processes and Devices (SISPAD) (2019). <https://doi.org/10.1109/SISPAD.2019.8870440>.
16. Bankapalli, Y. S., & Wong, H. Y., TCAD augmented machine learning for semiconductor device failure troubleshooting and reverse engineering. In: Proc. International Conference on Simulation of Semiconductor Processes and Devices (SISPAD), (2019). <https://doi.org/10.1109/SISPAD.2019.8870467>.
17. Mehta, K. *et al.* Improvement of TCAD augmented machine learning using autoencoder for semiconductor variation identification and inverse design. *IEEE Access* **8**, 143519–143529. <https://doi.org/10.1109/ACCESS.2020.3014470> (2020).
18. LeCun, Y., Bottou, L., Bengio, Y. & Haffner, P. Gradient-based learning applied to document recognition. *Proc. IEEE* **86**(11), 2278–2323. <https://doi.org/10.1109/5.726791> (1998).
19. Fukushima, K. Neocognitron: A self-organizing neural network model for a mechanism of visual pattern recognition. *Biol. Cybern.* **36**, 193–202. <https://doi.org/10.1007/BF00344251> (1980).
20. LeCun, Y. *et al.* Backpropagation applied to handwritten zip code recognition. *Neural Comput.* **1**(4), 541–551. <https://doi.org/10.1162/neco.1989.1.4.541> (1989).
21. Reda, I. *et al.* A new CNN-based system for early diagnosis of prostate cancer. 2018 IEEE 15th International Symposium on Biomedical Imaging (ISBI 2018), Washington, DC, USA, 2018, pp. 207–210, <https://doi.org/10.1109/ISBI.2018.8363556>.
22. Tang, S.-S., *et al.* Biomedical Image Edge Detection Based on CNN. 2017 International Conference on Wireless Communications, Networking and Applications, 84–88 (2017). <https://doi.org/10.1145/3180496.3180611>
23. Ronneberger, O., Fischer, P., Brox, T., U-Net: Convolutional Networks for Biomedical Image Segmentation, in Medical Image Computing and Computer-Assisted Intervention—MICCAI 2015, Lecture Notes in Computer Science, 9351. Springer, Cham. https://doi.org/10.1007/978-3-319-24574-4_28
24. Siddique, N., Paheding, S., Elkin, C. P. & Devabhaktuni, V. U-Net and its variants for medical image segmentation: A review of theory and applications. *IEEE Access* **9**, 82031–82057. <https://doi.org/10.1109/ACCESS.2021.3086020> (2021).
25. Rahman, T. *et al.* Exploring the effect of image enhancement techniques on COVID-19 detection using chest X-ray images. *Comput. Biol. Med.* **132**, 104319. <https://doi.org/10.1016/j.compbiomed.2021.104319> (2021).
26. Lee, W. J. *et al.* Device simulations with a U-Net model predicting physical quantities in two-dimensional landscapes. *Sci Rep* **13**, 731. <https://doi.org/10.1038/s41598-023-27599-z> (2023).
27. Chen, J., Viquerat, J., & Hachem, E., U-net architectures for fast prediction of incompressible laminar flows. arXiv, <https://arxiv.org/abs/1910.13532> (2019).

Acknowledgements

This work was financially supported by the “Center for the Advanced Semiconductor Technology Research” from The Featured Areas Research Center Program within the framework of the Higher Education Sprout Project by the Ministry of Education (MOE) in Taiwan. Also supported in part by the National Science and Technology Council (NSTC), Taiwan, under Grant 111-2622-8-A49-018-SB, 111-2221-E-492-022, 111-2221-E-492-012, and 112-2628-E-A49-020-MY3. The authors would like to thank the National Center for High-performance Computing of Taiwan for providing computational and storage resources.

Author contributions

B.-C. Chen, Y.-S. Hsiao, W.-C. Lin and T.-L. Wu drafted the manuscript. B.-C. Chen and Y.-S. Hsiao developed the model and prepared all the datasets. W.-J. Lee, N.-Y. Chen and T.-L. Wu supervised the research. All authors contributed to the discussion of the results and preparation of the manuscript.

Competing interests

The authors declare no competing interests.

Additional information

Correspondence and requests for materials should be addressed to W.-J.L., N.-Y.C. or T.-L.W.

Reprints and permissions information is available at www.nature.com/reprints.

Publisher's note Springer Nature remains neutral with regard to jurisdictional claims in published maps and institutional affiliations.



Open Access This article is licensed under a Creative Commons Attribution 4.0 International License, which permits use, sharing, adaptation, distribution and reproduction in any medium or format, as long as you give appropriate credit to the original author(s) and the source, provide a link to the Creative Commons licence, and indicate if changes were made. The images or other third party material in this article are included in the article's Creative Commons licence, unless indicated otherwise in a credit line to the material. If material is not included in the article's Creative Commons licence and your intended use is not permitted by statutory regulation or exceeds the permitted use, you will need to obtain permission directly from the copyright holder. To view a copy of this licence, visit <http://creativecommons.org/licenses/by/4.0/>.

© The Author(s) 2024